Static and Dynamic Analysis of Clamped Orthotropic Plates Using Lagrangian Multiplier Technique

P. C. Chen* and R. L. Ramkumar†
Northrop Corporation, Hawthorne, California

An analysis was developed to predict the static and dynamic response of clamped orthotropic laminates. The dynamic loading conditions included low-velocity impact by a hard object. Shear deformation effects in the clamped plate were accounted for using a higher-order plate theory. The natural frequencies and the corresponding mode shapes were computed by solving the eigenvalue problem using Lagrangian multiplier technique. The dynamic analysis incorporated the static response and the eigenvalue solutions into the mode acceleration technique. The static and dynamic analyses were validated by demonstrating a good correlation between the calculated results, available experimental data, and other analytical results. The validated analysis was used to predict the damage introduced in clamped orthotropic plates due to low-velocity impact by a hard object.

Nomenclature

a = length of the plate
A_{ij} = inplane stiffness
b = width of the plate
c = contact time of the forcing function
D_{ij} = bending stiffness
g = acceleration due to gravity
h = thickness of the plate
u, v = length and width of the impact area, respectively
α, β = Lagrange multipliers
ξ, η = impact location
γ = laminate weight density
ω = natural frequency

Subscripts
k = kth mode
l = lth mode
$,x; ,y; ,t$ = derivatives of ( )

Introduction

THE past decade has witnessed considerable interest in the analytical and experimental investigation of the effect of low-velocity impact on laminated plates.[1-13] Test results indicate that, under possible impact threat conditions, laminated structural components can suffer a significant (nearly 60%) compressive strength loss, without any visible indication of the damage on the impacted surface.[10,12,13] This is, therefore, a problem of considerable interest to researchers and of considerable concern to designers and possesses the potential to influence the design allowables for compressively loaded structural components.

While a large amount of experimental data is available, only restrictively validated analyses are being developed to predict the extent of damage in, and the residual strength of, laminates subjected to low-velocity impact loading. The analytical difficulties are introduced by many factors: 1) the general anisotropy of the laminate, 2) the constraint condition at the laminate boundaries, 3) the complex contact problem that necessitates an incremental-iterative analytical procedure, 4) the predominant interlaminar failures that cannot be predicted using the classical laminated plate theory, and 5) the complexity involved in predicting the residual strength of a laminate containing multiple delaminations and intraply failures.

The dynamic analysis of a laminated plate involves the computation of its natural frequencies and mode shapes. This task can be performed in closed form only when the plate is isotropic or specially orthotropic and is constrained by simple supports at the boundaries.[14,15] The problem increases in complexity when the plate exhibits general anisotropy. In this case, even when the boundaries are simple supports, one must resort to approximate analytical procedures. If the boundaries are clamped, approximate solutions are the only possibility, even for isotropic plates. And, if the plate thickness is not negligible in comparison to planform dimensions, shear deformation effects have to be accounted for, necessitating a higher-order analysis.[16,17]

In the program reported here, a dynamic analysis was developed to predict the forced response of clamped orthotropic plates. The dynamic analysis incorporates results from a static analysis and an eigenvalue problem (natural frequencies and mode shapes) into a mode acceleration solution scheme.[18] The reader is referred to Refs. 19 and 20 for the eigenvalue solutions obtained using the Lagrangian multiplier technique. The static analysis, also performed using the Lagrangian multiplier method, and the dynamic analysis are described below.

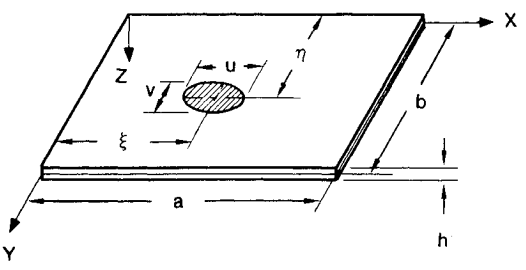

Fig. 1 Geometry, reference coordinates, and semiellipsoidal load distribution details for clamped laminates; impactor also shown.

Received Aug. 30, 1985; revision received April 16, 1986; presented as Paper 86-0932 at the AIAA/ASME/ASCE/AHE 27th Structures, Structural Dynamics and Materials Conference, San Antonio, TX, May 19-21, 1986.

*Engineering Specialist, Composite Manufacturing Technology, Aircraft Division.

†Manager, Composite Manufacturing Technology, Aircraft Division.

Static Analysis

Consider a semiellipsoidal load distribution on a clamped laminated plate (Fig. 1). The length, width, and thickness dimensions of the plate are a, b, and h, respectively. The plate displacements along the reference x, y, and z directions are $\bar{u}$, $\bar{v}$, w, respectively. ψ_x and ψ_y are the plate midplane bending shapes in the xz and yz planes, respectively. The laminate is assumed to be midplane symmetric, and its midplane translations are assumed to be negligible in comparison to the flexure-induced displacements. Transverse shear deformation effects are accounted for using a higher-order plate theory,[16,17] assuming a Mindlin shear correction factor K of $\pi^2/12$. In this case, the plate response is defined in terms of its three variables (w, ψ_x, and ψ_y), their derivatives ($w_{,x}$, $\psi_{x,y}$, etc.), and the laminate in-plane and bending stiffnesses (A_{ij} and D_{ij}, respectively, as described in Ref. 15, for $i, j = 1,2,6$). The reader is referred to Ref. 16 for the appropriate expressions. For an orthotropic laminate, $D_{16} = D_{26} = 0$.

The expression for the total strain energy V in the considered laminate is

$$\begin{aligned} V = \tfrac{1}{2}\int\int_{\text{area}} \Big[& KA_{44}(w_{,y}+\psi_y)^2 + KA_{55}(w_{,x}+\psi_x)^2 \\ & + 2KA_{45}(w_{,x}w_{,y} + w_{,x}\psi_y + w_{,y}\psi_x + \psi_x\psi_y) \\ & + D_{11}\psi_{x,x}^2 + 2D_{12}\psi_{x,x}\psi_{y,y} + D_{22}\psi_{y,y}^2 \\ & + 2D_{16}\psi_{x,x}(\psi_{x,y}+\psi_{y,x}) + 2D_{26}\psi_{y,y}(\psi_{x,y}+\psi_{y,x}) \\ & + D_{66}(\psi_{x,y}+\psi_{y,x})^2\Big]\,\mathrm{d(area)} \end{aligned} \tag{1}$$

The work done by an externally applied load (P per unit area) is

$$Q = \int_0^a\int_0^b P(x,y,t)\,W(x,y,t)\,\mathrm{d}x\,\mathrm{d}y \tag{2}$$

When the applied load is a static load, P and W are independent of time t. For the semiellipsoidal load distribution in Fig. 1, let P_T be the total applied load. The work done by this load is

$$\begin{aligned} Q = {} & P_0\int_{x_1}^{x_2}\int_{y_1}^{y_2}\left[1 - \frac{(x-\xi)^2}{u^2} - \frac{(y-\eta)^2}{v^2}\right]^{1/2} \\ & \times\left[\sum_m\sum_n a_{mn}\sin\left(\frac{m\pi x}{a}\right)\sin\left(\frac{n\pi y}{b}\right)\right]\mathrm{d}x\,\mathrm{d}y \end{aligned} \tag{3}$$

where

$$\begin{aligned} & P_0 = 3P_T/(2\pi uv), \qquad x_1 = \xi - u, \qquad x_2 = \xi + u \\ & y_1 = \eta - v\left[1 - (x-\xi)^2/u^2\right]^{\frac{1}{2}} \\ & y_2 = \eta + v\left[1 - (x-\xi)^2/u^2\right]^{\frac{1}{2}} \end{aligned} \tag{4}$$

Equation (3) can be rewritten as

$$Q = \sum_m\sum_n q_{mn}a_{mn} \tag{5}$$

where q_{mn} is defined as

$$\begin{aligned} q_{mn} = {} & P_0\int_{x_1}^{x_2}\int_{y_1}^{y_2}\left[\frac{1-(x-\xi)^2}{u^2} - \frac{(y-\eta)^2}{v^2}\right]^{1/2} \\ & \times\sin\left(\frac{m\pi x}{a}\right)\sin\left(\frac{n\pi y}{b}\right)\mathrm{d}x\,\mathrm{d}y \end{aligned} \tag{6}$$

While an analytical solution for Eq. (6) is difficult to obtain, a numerical solution may be computed using, say, the Gaussian quadrature approach.

The following boundary conditions apply to the clamped plate in Fig. 1:

$$w(0,y,t) = w(a,y,t) = w(x,0,t) = w(x,b,t) = 0 \tag{7}$$

$$\psi_x(0,y,t) = \psi_x(a,y,t) = \psi_y(x,0,t) = \psi_y(x,b,t) = 0 \tag{8}$$

The following series expressions are assumed for the plate variables:

$$w(x,y,t) = \sum_m^\infty\sum_n^\infty a_{mn}\sin\left(\frac{m\pi x}{a}\right)\sin\left(\frac{n\pi y}{b}\right)Z(t) \tag{9}$$

$$\psi_x(x,y,t) = \sum_m^\infty\sum_n^\infty b_{mn}\cos\left(\frac{m\pi x}{a}\right)\sin\left(\frac{n\pi y}{b}\right)Z(t) \tag{10}$$

$$\psi_y(x,y,t) = \sum_m^\infty\sum_n^\infty d_{mn}\sin\left(\frac{m\pi x}{a}\right)\cos\left(\frac{n\pi y}{b}\right)Z(t) \tag{11}$$

where a_{mn}, b_{mn}, and d_{mn} are unknown coefficients and $Z(t) = 1$ for the static problem. Equation (9) satisfies the clamped boundary displacement conditions, but Eqs. (10) and (11) do not satisfy the zero-slope conditions at the boundary. The following constraint conditions must be satisfied to impose the unsatisfied zero slope boundary conditions:

$$\sum_m^\infty b_{mj} = 0, \qquad j = 1,2,3,\ldots q \tag{12}$$

$$\sum_n^\infty d_{in} = 0, \qquad i = 1,2,3,\ldots p \tag{13}$$

Introducing Lagrange multipliers for the above constraint conditions,[20] the function to be minimized becomes

$$G = V + Q - \sum_{j=1}^{q}\left(\alpha_j\sum_{m=1}^{\infty}b_{mj}\right) - \sum_{i=1}^{p}\left(\beta_i\sum_{n=1}^{\infty}d_{in}\right) \tag{14}$$

Substituting Eqs. (9-11) into Eq. (1), the expression for V becomes

$$\begin{aligned} V = {} & (ab\pi^2/4)\sum_m^\infty\sum_n^\infty\big[E_{mn}a_{mn}^2 + F_{mn}b_{mn}^2 + G_{mn}d_{mn}^2 \\ & + 2H_m a_{mn}b_{mn} + 2U_n a_{mn}d_{mn} + 2Q_{mn}b_{mn}d_{mn}\big] \end{aligned} \tag{15}$$

where

$$\begin{aligned} E_{mn} &= (K/2)\left[A_{44}(n/b)^2 + A_{55}(m/a)^2\right] \\ F_{mn} &= \tfrac{1}{2}\left[KA_{55}/\pi^2 + D_{11}(m/a)^2 + D_{66}(n/b)^2\right] \\ G_{mn} &= \tfrac{1}{2}\left[KA_{44}/\pi^2 + D_{22}(n/b)^2 + D_{66}(m/a)^2\right] \\ H_m &= (K/2\pi)A_{55}(m/a) \\ U_n &= (K/2\pi)A_{44}(n/b) \\ Q_{mn} &= \tfrac{1}{2}(D_{12}+D_{66})(m/a)(n/b) \end{aligned} \tag{16}$$

The minimization equations are[20]

$$\frac{\partial G}{\partial a_{mn}} = \frac{\partial G}{\partial b_{mn}} = \frac{\partial G}{\partial d_{mn}} = 0\ (m,n = 1,2,3\ldots) \tag{17}$$

Writing the above equations in matrix form, one obtains:

$$\begin{bmatrix} E_{mn} & H_m & U_n \\ H_m & F_{mn} & Q_{mn} \\ U_n & Q_{mn} & G_{mn} \end{bmatrix} \begin{Bmatrix} a_{mn} \\ b_{mn} \\ d_{mn} \end{Bmatrix} = \left(\frac{2}{ab\pi^2}\right) \begin{Bmatrix} q_{mn} \\ \alpha_n \\ \beta_n \end{Bmatrix} \tag{18}$$

These equations provide the following solutions for a_{mn}, b_{mn}, and d_{mn}:

$$a_{mn} = (2/ab\pi^2)\left[q_{mn}(F_{mn}G_{mn} - Q_{mn}^2) + \alpha_n(U_nQ_{mn} - G_{mn}H_m) + \beta_m(H_mQ_{mn} - F_{mn}U_n)\right]/\Delta_{mn} \tag{19}$$

$$b_{mn} = (2/ab\pi^2)\left[q_{mn}(U_nQ_{mn} - G_{mn}H_m) + \alpha_n(E_{mn}G_{mn} - U_n^2) + \beta_m(H_mU_n - E_{mn}Q_{mn})\right]/\Delta_{mn} \tag{20}$$

$$d_{mn} = (2/ab\pi^2)\left[q_{mn}(H_mQ_{mn} - F_{mn}U_n) + \alpha_n(H_mU_n - E_{mn}Q_{mn}) + \beta_m(E_{mn}F_{mn} - H_m^2)\right]/\Delta_{mn} \tag{21}$$

where

$$\Delta_{mn} = E_{mn}(F_{mn}G_{mn} - Q_{mn}^2) - H_m(H_mG_{mn} - U_nQ_{mn}) + U_n(H_mQ_{mn} - U_nF_{mn}) \tag{22}$$

In Eqs. (19-21), α_n is not present when $n > q$ and β_m is not present when $m > p$. Substituting Eqs. (20) and (21) into the constraint conditions [Eqs. (12) and (13)], one obtains

$$\alpha_j \sum_m^{\infty} (E_{mj}G_{mj} - U_j^2)/\Delta_{mj} + \sum_m^{p} (H_mU_j - E_{mj}Q_j)\beta_m/\Delta_{mj} = -\sum_m^{\infty} q_{mj}(U_jQ_{mj} - G_{mj}H_m)/\Delta_{mj} \quad (j = 1,2,3,\ldots q) \tag{23}$$

$$\sum_n^{q} (H_iU_n - E_{in}Q_{in})\alpha_n/\Delta_{in} + \beta_i \sum_n^{\infty} (E_{in}F_{in} - H_i^2)/\Delta_{in} = -\sum_n^{\infty} q_{in}(H_iQ_{in} - F_{in}U_n)/\Delta_{in} \quad (i = 1,2,3\ldots p) \tag{24}$$

Equations (23) and (24) yield $p + q$ linear equations for $p + q$ unknowns: $\alpha_1, \alpha_2, \ldots, \alpha_q$, $\beta_1, \beta_2, \ldots, \beta_{p-1}$, and β_p. Solving these equations and substituting the results into Eqs. (19–21), the coefficients a_{mn}, b_{mn}, and d_{mn} are computed. The transverse displacement and bending slope variations over the plate are then computed using Eqs. (9), (10), and (11). The strains in the various plies and the transverse shear stress resultants are computed using the expressions in Ref. 16.

Dynamic Analysis

The governing equations of motion for an orthotropic plate, ignoring rotatory inertia effects are[8]

$$KA_{55}\Psi_{x,x} + KA_{55}W_{,xx} + KA_{44}\Psi_{y,y} + KA_{44}W_{,yy} = (\gamma h/g)W_{,tt} - P(x,y,t) \tag{25}$$

$$D_{11}\Psi_{x,xx} + D_{66}\Psi_{x,yy} + (D_{12} + D_{66})\Psi_{y,xy} - KA_{55}(\Psi_x + W_{,x}) = 0 \tag{26}$$

$$(D_{12} + D_{66})\Psi_{x,xy} + D_{66}\Psi_{y,xx} + D_{22}\Psi_{y,yy} - KA_{44}(\Psi_y + W_{,y}) = 0 \tag{27}$$

Reference 20 describes how the natural frequencies and corresponding mode shapes are obtained for each set of m and n values. These essentially correspond to the solution of the following equations:

$$KA_{55}(\Psi_{x,x})_k + KA_{55}(W_{,xx})_k + KA_{44}(\Psi_{y,y})_k + KA_{44}(W_{,yy})_k = -\omega_k^2(\gamma h/g)(W)_k \tag{28}$$

$$D_{11}(\Psi_{x,xx})_k + D_{66}(\Psi_{x,yy})_k + (D_{12} + D_{66})(\Psi_{y,xy})_k - KA_{55}(\Psi_x + W_{,x})_k = 0 \tag{29}$$

$$(D_{12} + D_{66})(\Psi_{x,xy})_k + D_{66}(\Psi_{y,xx})_k + D_{22}(\Psi_{y,yy})_k - KA_{44}(\Psi_y + W_{,y})_k = 0 \tag{30}$$

where $(W)_k$, $(\Psi_x)_k$, and $(\Psi_y)_k$ are the mode shapes corresponding to the natural frequency ω_k. If k and l represent two sets of m and n values, the orthogonality condition for the principal modes may be written as[8]

$$(\omega_k^2 - \omega_l^2)\int_0^a \int_0^b \left(\frac{\gamma h}{g}\right)(W)_k(W)_l \,dx\,dy = 0 \tag{31}$$

where the integral is zero when $k \neq l$.

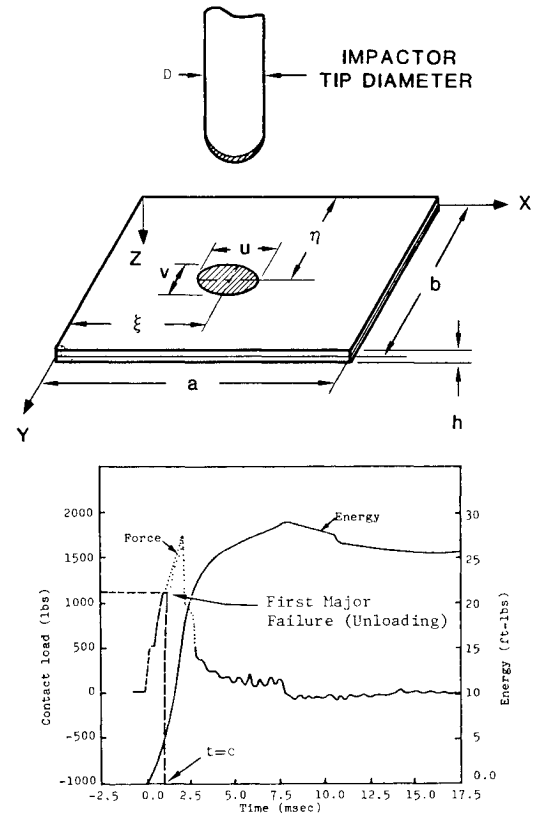

Fig. 2 Typical contact force/absorbed energy variation with time.

The solutions to the dynamic problem [Eqs. (25-27)] can be separated into functions of position and time as follows:

$$W(x,y,t)=\sum_{k}^{\infty}(W)_k Z_k(t)$$

$$\Psi_x(x,y,t)=\sum_{k}^{\infty}(\Psi_x)_k Z_k(t)$$

$$\Psi_y(x,y,t)=\sum_{k}^{\infty}(\Psi_y)_k Z_k(t) \tag{32}$$

where the kth mode shapes are defined as follows [(Eqs. 9-11)]:

$$(W)_k=\sum_m\sum_n(a_{mn})_k\sin\left(\frac{m\pi x}{a}\right)\sin\left(\frac{n\pi y}{b}\right)$$

$$(\Psi_x)_k=\sum_m\sum_n(b_{mn})_k\cos\left(\frac{m\pi x}{a}\right)\sin\left(\frac{n\pi y}{b}\right)$$

$$(\Psi_y)_k=\sum_m\sum_n(d_{mn})_k\sin\left(\frac{m\pi x}{a}\right)\cos\left(\frac{n\pi y}{b}\right) \tag{33}$$

and $Z_k(t)$ is a time-dependent generalized coordinate.

Substituting Eq. (32) into Eqs. (25-27) and using Eqs. (28-30), one obtains

$$-\sum_{k}^{\infty}\omega_k^2(W)_k Z_k+\frac{P}{\gamma h/g}=\sum_{k}^{\infty}(W)_k(Z_{,tt})_k \tag{34}$$

Expanding $P(x,y,t)$ in terms of the generalized forces $T_k(t)$ as

$$\frac{P}{\gamma h/g}=\sum_{k}^{\infty}T_k(t)(W)_k \tag{35}$$

Eq. (34) may be written as follows, for every k:

$$[Z_{,tt}(t)]_k+\omega_k^2 Z_k(t)=T_k(t) \tag{36}$$

where

$$T_k(t)=\frac{\int_0^a\int_0^b P(x,y,t)(W)_k\,dx\,dy}{(\gamma h/g)\int_0^a\int_0^b(W)_k^2\,dx\,dy} \tag{37}$$

Equation (37) is obtained by multiplying Eq. (35) by $(\gamma h/g)(W)_l$ and integrating the product over the plate area using Eq. (31).

For zero initial displacement and velocity, the solution to Eq. (36) is

$$Z_k(t)=\left(\frac{1}{\omega_k}\right)\int_0^t T_k(\tau)\sin\omega_k(t-\tau)\,d\tau \tag{38}$$

Assuming the applied load to be separable in space and time, $P(x,y,t)=P(x,y)\,f(t)$. If the load is assumed to be semiellipsoidal in distribution, Eq. (5) may be used for the numerator in Eq. 37. This yields

$$T_k(t)=\frac{\left[\sum_m\sum_n(a_{mn})_k q_{mn}\right]f(t)}{(\gamma h/g)(ab/4)\sum_m\sum_n(a_{mn})_k^2} \tag{39}$$

where q_{mn} is defined in Eq. (6). Substituting this expression into Eq. (38) yields

$$Z_k(t)=\frac{\sum_m\sum_n(a_{mn})_k q_{mn}}{\omega_k(\gamma h/g)(ab/4)\sum_m\sum_n(a_{mn})_k^2}\times\int_0^t f(\tau)\sin\omega_k(t-\tau)\,d\tau \tag{40}$$

The time dependence of the applied load $f(t)$ is assumed to be known. Incorporation of Eq. (40) into Eq. (32) provides the solutions to the dynamic problem. Substituting these solutions into the appropriate expressions in Ref. 16, the strain state and the transverse shear stress resultants in the clamped plate are obtained.

The above procedure converges slowly and may require a considerable amount of computer time to achieve solution accuracy. To overcome this difficulty, the mode acceleration method is used.[18] Equation (35) is rearranged as follows:

$$Z_k(t)=T_k(t)/\omega_k^2-Z_{k,tt}(t)/\omega_k^2 \tag{41}$$

Substituting Eqs. (39) and (40) into Eq. (41) and substituting the result into Eq. (32), one obtains

$$W(x,y,t)=W_s(x,y)f(t)-\sum_{k=1}^{\infty}\left\{\left[\frac{\sum_m\sum_n(a_{mn})_k q_{mn}}{\omega_k^3(\gamma g/h)(ab/4)\sum_m\sum_n(a_{mn})_k^2}\right]\times\left[\sum_m\sum_n(a_{mn})_k\sin\left(\frac{m\pi x}{a}\right)\sin\left(\frac{n\pi y}{b}\right)\right]\frac{d^2}{dt^2}\times\int_0^t f(\Upsilon)\sin\omega_k(t-\Upsilon)\,d\Upsilon\right\} \tag{42}$$

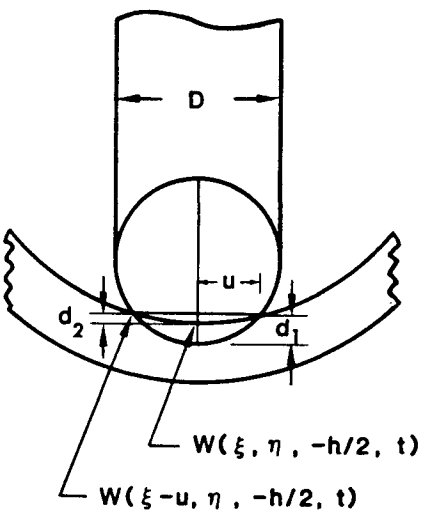

Depth of indentation = $d_1 - d_2$

where: $d_1 = 0.5\,[D-(D^2-4u^2)^{\frac{1}{2}}]$

$d_2 = W(\xi,\eta,-h/2,t) - W(\xi-u,\eta,-h/2,t)$

Fig. 3 Impactor and plate displacements and depth of indentation.

$$\psi_x(x,y,t) = \psi_{xs}(x,y)f(t) - \sum_{k=1}^{\infty}\left\{\left[\frac{\sum\sum(a_{mn})_k q_{mn}}{\omega_k^3(\gamma g/h)(ab/4)\sum\sum(a_{mn})_k^2}\right] \times\left[\sum\sum(b_{mn})_k\cos\left(\frac{m\pi x}{a}\right)\sin\left(\frac{n\pi y}{b}\right)\right]\frac{d^2}{dt^2} \times\int_0^t f(\Upsilon)\sin\omega_k(t-\Upsilon)\,d\Upsilon\right\} \quad (43)$$

$$\psi_y(x,y,t) = \psi_{ys}(x,y)f(t) - \sum_{k=1}^{\infty}\left\{\left[\frac{\sum\sum(a_{mn})_k q_{mn}}{\omega_k^3(\gamma g/h)(ab/4)\sum\sum(a_{mn})_k^2}\right] \times\left[\sum\sum(d_{mn})_k\sin\left(\frac{m\pi x}{a}\right)\cos\left(\frac{n\pi y}{b}\right)\right]\frac{d^2}{dt^2} \times\int_0^t f(\Upsilon)\sin\omega_k(t-\Upsilon)\,d\Upsilon\right\} \quad (44)$$

where $W_s(x,y)$, $\psi_{xs}(x,y)$, and $\psi_{ys}(x,y)$ are the solutions to the static problem, corresponding to a static load $P(x,y)$ obtained by substituting Eq. (39) into Eq. (35). For example,

$$W_s(x,y) = \sum_{k=1}^{\infty}\left[\frac{\sum\sum(a_{mn})_k q_{mn}}{\omega_k^2(\gamma g/h)(ab/4)\sum\sum(a_{mn})_k^2}\right] \times\sum\sum(a_{mn})_k\sin\left(\frac{m\pi x}{a}\right)\sin\left(\frac{n\pi y}{b}\right) \quad (45)$$

This static solution is obtainable using the mode superposition method. However, the static solutions have already been derived earlier using the Lagrangian multiplier method.

Comparing Eq. (42) with Eq. (40), it is seen that ω_k^3 is present in the denominator of Eq. (42), while only ω_k is present in the denominator of Eq. (40). As the higher-order modes (with larger ω_k values) are accounted for, this causes the mode acceleration method to converge quickly to the accurate solution.

Results

Static and dynamic loads are applied to two clamped graphite/epoxy laminates. The laminates have the same layup with different cured ply thicknesses.[9] Their geometric and material properties[11] are listed in Table 1. D_{16} and D_{26} for the two laminates are less than 5% of the other D_{ij} values. Therefore, the two laminates are nearly orthotropic ($D_{16} = D_{26} = 0$).

The static problem assumes a concentrated (point) unit load to be applied at the center $(a/2, b/2, -h/2)$ of the 25 × 9 in. clamped laminates. In this case, the expression for q_{mn} in Eq. (6), corresponding to a semiellipsoidal load distribution, is replaced by[8]

$$q_{mn} = (4P_T/ab)\sin(m\pi\xi/a)\sin(n\pi\eta/b) \quad (46)$$

where $P_T = 1$ (unit load), $\xi = a/2$, and $\eta = b/2$ (see Fig. 1). Table 2 compares the predictions of the developed Lagrangian multiplier solution with those based on a Rayleigh-Ritz solution.[21] It is seen that, when shear deformation effects are not accounted for,[22] the Rayleigh-Ritz solutions are 10 and 23% lower than the developed Lagrangian multiplier solutions for plates A and B, respectively. The thicker laminate B exhibits a significant shear deformation effect on the transverse plate displacement. If the transverse shear stiffnesses (A_{44} and A_{55}) in the Lagrangian multiplier solution are increased by a factor of 1000, the predictions are within 5% of the Rayleigh-Ritz solution.

The dynamic loading conditions[8,11] considered are listed in Table 3. The clamped laminates are subjected to low-velocity impact by a hard (steel) object (see Fig. 2). The forcing function is obtained through instrumented impact tests.[9] The first major damage (generally a delamination) occurs at $t = c$. The elliptical contact area at $t = c$, defined by u and v, is dependent on the impactor tip diameter D. The u and v values in Table 3 are obtained from contact damage measurements.[8,11] The depth of indentation is dependent on D, u, v, and the plate displacement w, as shown in Fig. 3.

The computed dynamic response of the clamped plates is based on an assumed semiellipsoidal load distribution, the eigenvalue solutions from Ref. 20, and the developed solution

Table 1 Geometry and properties of analyzed graphite/epoxy laminates

Property		Laminate A[a]	Laminate B[a]
h,	in.	0.25	0.5
D_{11},	lb-in.	1.453×10^4	1.1627×10^5
D_{12},	lb-in.	3.74×10^3	2.9929×10^4
D_{16},	lb-in.	1.86×10^2	1.4876×10^3
D_{22},	lb-in.	6.415×10^3	5.1323×10^4
D_{26},	lb-in.	1.86×10^2	1.4876×10^3
D_{66},	lb-in.	4.032×10^3	3.2359×10^4
A_{55},	lb-in.	1.9968×10^5	3.9936×10^5
A_{44},	lb-in.	1.9968×10^5	3.9936×10^5
K		0.8225	0.8225
γ,	lb-in.	0.68914	0.68914
h_{ply}	in.	0.0052	0.0104
a,	in.	25.0	25.0
b,	in.	9.0	9.0

[a] Laminates A and B are 48-ply laminates with the following layup $[(\pm 45/0_2)_2/\pm 45/0/90]_{2s}$. h_{ply} is the individual ply thickness of the AS1/3501-6 graphite/epoxy prepreg. It is 0.0052 and 0.014 in. for laminates A and B, respectively.

Table 2 Central deflection (in.) predictions of clamped laminates due to a unit static load applied at the center $(a/2, b/2, -h/2)$

	Developed Lagrangian multiplier solution		Rayleigh-Ritz solution
Laminate[a]	With shear deformation[b]	Without shear deformation[b,c]	Without shear deformation
A	7.52×10^{-5}	7.08×10^{-5}	6.76×10^{-5}
B	1.10×10^{-5}	8.85×10^{-6}	8.44×10^{-6}

[a] 25 × 9 in. laminates (see Table 1). [b] $p = q = 15$; $m, n = 1, 2, \ldots, 30$. [c] The actual A_{44} and A_{55} values in Table 1 were multiplied by 1000.

using the accelerated mode method. Figures 4 and 5 present sample plate displacement predictions for an off-center impact situation (test case 2 in Table 3). These, in conjunction with the information in Table 3, are used to compute the impactor tip displacement as shown in Fig. 3. Table 4 indicates that the analysis predicts plate displacements that are approximately 25% smaller than those predicted by the analysis in Ref. 11. This is because the Fourier transform technique in Ref. 11 does not explicitly impose the clamped boundary conditions at the finite-boundary locations. Table 4 also indicates that the predicted impactor tip displacements for the various test cases, at $t = c$, are in good agreement with the measured values.[9]

Sample predictions of the transient strain variations in the impacted laminates are presented in Figs. 6 and 7. Table 5 lists the maximum strains at $t = c$, predicted using the developed analysis and the analysis in Ref. 11 and measured experimentally in Ref. 9. It is seen that this analysis demonstrates a better correlation with the test results[9] than the analysis in Ref. 11.

Sample predictions of the longitudinal and transverse averaged interlaminar shear strains (Q_x/h and Q_y/h, respectively) are presented in Figs. 8 and 9. The curves corresponding to $t = c$ are used in conjunction with assumed, albeit arbitrary, failure values for Q_x/h and Q_y/h to predict the extent of internal damage.[11] Using a failure value of 2 ksi for Q_x/h and Q_y/h, the developed analysis predicted the delamination size at $t = c$. Table 6 compares the predicted delamination sizes with those measured using ultrasonic equipment.[9] In reality, the damage state in the impacted laminate is complex (delaminations, intraply failures, contact damage, etc.). The delamination predictive procedure in Refs. 8 and 11 is rather simple-minded and is constrained by the limitations of the employed higher-order plate theory. Nevertheless, the assumed failure values for Q_x/h and Q_y/h predict delamination sizes that correlate well with the ultrasonic C-scan measurements in Ref. 9.

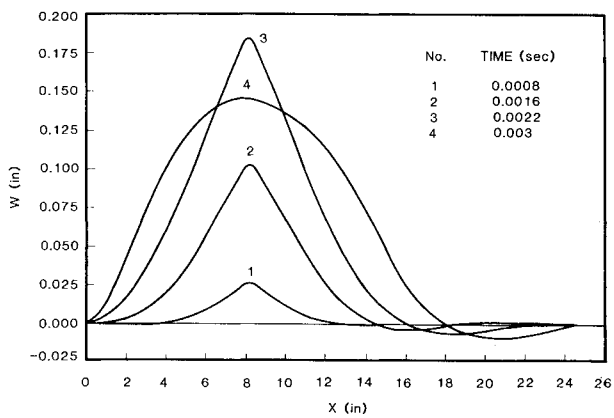

Fig. 4 Predicted $W(x, \eta, 0, t)$ for test case 2.

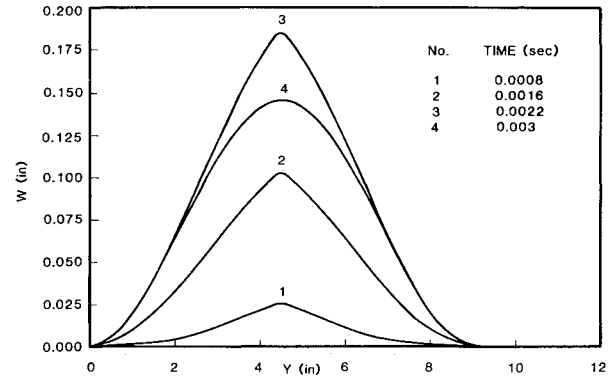

Fig. 5 Predicted $W(\xi, y, 0, t)$ for test case 2.

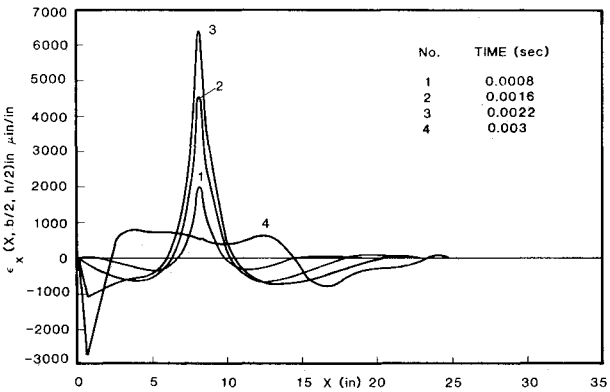

Fig. 6 Predicted $\epsilon_x(x, \eta, -h/2, t)$ for test case 2.

Table 3 Contact time, force, and area information for considered dynamic problem[a]

Test case	Laminate	Impactor D, in.	P_T at $t = c$, in.	c, s	ξ, in.	η, in.	$u = v$ in.
1	A	0.125	1.150	0.00125	3.833	4.5	0.005
2	A	0.5	2.772	0.0022	8.166	4.5	0.125
3	A	2.0	3.264	0.0024	12.5	4.5	0.35
4	B	0.5	6.563	0.00125	8.166	4.5	0.125
5	B	2.0	8.642	0.0145	12.5	4.5	0.35

[a]See Fig. 2 for a definition of the listed variables.

Table 4 Plate and impactor displacements at $t = c$

Test case (Table 3)	$W(\zeta, \eta, -h/2, c)$ in. Developed analysis[a]	$W(\zeta, \eta, -h/2, c)$ in. Ref. 11	Impactor tip displacement, in. at $t = c$ Developed analysis[a]	Impactor tip displacement, in. at $t = c$ Experimental measurement (Ref. 9)
1	0.044	0.0818	0.106	0.1
2	0.1832	0.225	0.2152	0.22
3	0.226	0.277	0.284	0.25
4	0.06755	0.0818	0.10045	0.122
5	0.0938	0.12013	0.1527	0.136

[a]$p = q = 15$; $m, n = 1, 2, \ldots, 30$.

Table 5 Maximum strains in the impacted laminates at $t = c$

Test case (Table 3)	$\epsilon_x(\xi, \eta, -h/2, c)$, μin./in. Developed analysis[a]	ϵ_x Analysis in Ref. 11	ϵ_x Experimental measurement (Ref. 9)	$\epsilon_y(\xi, \eta, -h/2, c)$, μin./in. Developed analysis[a]	ϵ_y Analysis in Ref. 11	ϵ_y Experimental measurement (Ref. 9)
1	2622	2850	2318	4659	4650	4789
2	6348	7252	6182	12930	11851	12000
3	6737	6725	5455	12560	10331	16000
4	3572	4052	4364	8190	7329	8364
5	4285	4500	—	9040	7500	—

[a]$p = q = 15$; $m, n = 1, 2, \ldots 30$.

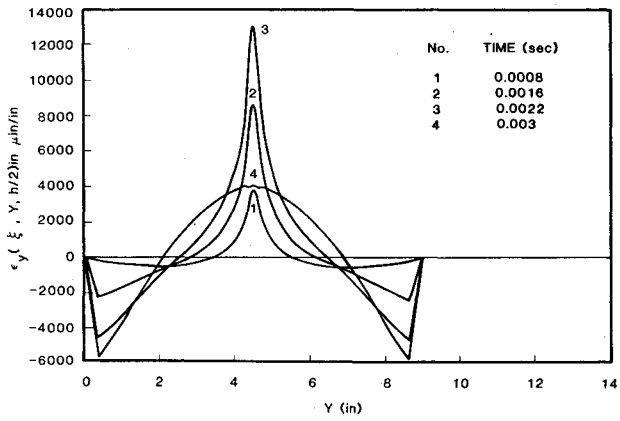

Fig. 7 Predicted $\epsilon_y(\xi, y, -h/2, t)$ for test case 2.

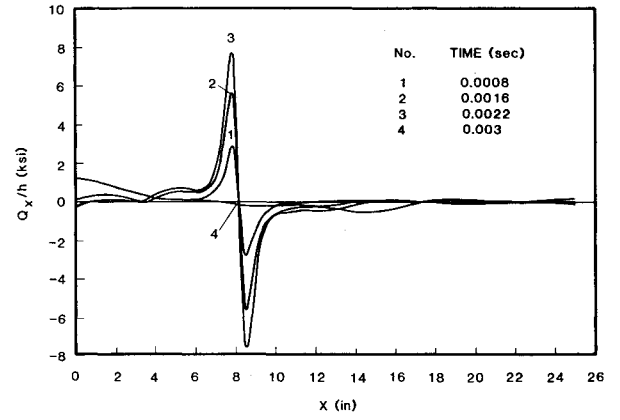

Fig. 8 Predicted $Q_x(x, \eta, t)/h$ for test case 2.

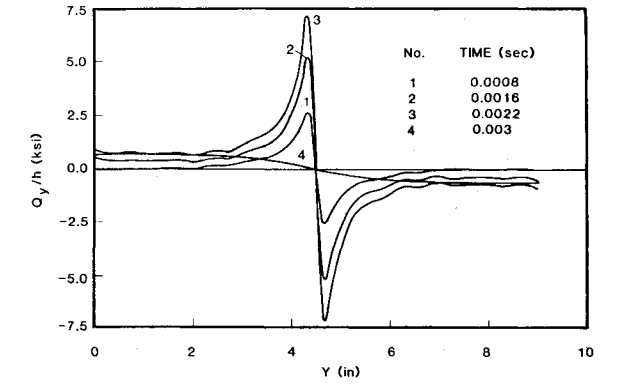

Fig. 9 Predicted $Q_y(\xi, y, t)/h$ for test case 2.

Table 6 Delamination size at $t = c$

Test case (Table 3)	Delamination diameter, in.	
	Developed analysis[a]	Experimental measurement (Ref. 9)
1	0.37	0.37
2	2.00	1.63
3	3.00	3.67

[a]Failure values of Q_x/h and Q_y/h were assumed to be 2 ksi. $p = q = 15$; $m, n = 1, 2, \ldots, 30$.

Conclusions

An analysis was developed to predict the dynamic response of clamped orthotropic plates. The analysis incorporated a static solution and a free vibration (eigenvalue) solution obtained using the Lagrangian multiplier method into a dynamic solution based on the mode acceleration technique. The developed solutions accounted for shear deformation effects through a higher-order plate theory. The static solution was validated by comparing predictions with those based on a Rayleigh-Ritz approach. The eigenvalue analysis had been validated earlier by establishing a good correlation between its predictions, available test results, and Rayleigh-Ritz solutions. The developed dynamic solution was validated by applying it to a low-velocity impact situation. Analytical predictions of the displacements and strains in the impacted laminates correlated well with the experimental measurements. The analysis was also successfully used, albeit in conjunction with an invalidated failure criterion, to predict the extent of internal damage (delamination) in the impacted laminates.

Acknowledgment

The work reported here was performed as an Independent Research and Development activity in the Strength and Life Assurance Research Organization at the Northrop Aircraft Division.

References

[1]McQuillen, E.J., Llorens, R.E., and Gause, L.W., "Low Velocity Transverse Normal Impact of Graphite-Epoxy Composite Laminates," Naval Air Development Center, Rept. 75119-30, June 1974.

[2]Sun, C.T. and Whitney, J.M., "Dynamic Response of Laminated Composite Plates Under Initial Stress," *AIAA Journal*, Vol. 14, Feb. 1976, pp. 268-270.

[3]Sun, C.T. and Chattopadhyay, S., "Dynamic Response of Anisotropic Laminated Plates under Initial Stress to Impact of a Mass," AFML-TR-74-258, March 1976.

[4]Starnes, J.H. Jr., Rhodes, M.D., and Williams, J.G., "The Effect of Impact Damage and Circular Holes on the Compressive Strength of a Graphite-Epoxy Laminate," NASA TM 78796, Oct. 1978.

[5]Chou, P.C., Flis, W.J., and Miller, H., "Certification of Composite Aircraft Structures Under Impact, Fatigue and Environmental Conditions; Part I—Low Speed Impact of Plates of Composite Materials," Naval Air Development Center, Rept. 78259-60, Jan. 1978.

[6]Bhatia,.M., "Impact Damage Tolerance of Thick Graphite-Epoxy Laminates," Naval Air Development Center, Rept. 7938-60, Jan. 1979.

[7]Byers, B.A., "Behavior of Damaged Graphite-Epoxy Laminates Under Compression Loading," NASA 159293, Aug. 1980.

[8]Dobyns, A.L., "Analysis of Simply-Supported Orthotropic Plates Subject to Static and Dynamic Loads," *AIAA Journal*, Vol. 19, May 1981, pp. 642-650.

[9]Ramkumar, R.L., "Composite Impact Damage Susceptibility," Naval Air Development Center, Rept. 79068-60, Jan. 1981.

[10]Ramkumar, R.L., "Environmental Effects on Composite Damage Criticality," Naval Air Development Center, Rept. 79067-60, Jan. 1982.

[11]Ramkumar, R.L. and Chen, P.C., "Low Velocity Impact Response of Laminated Plates," *AIAA Journal*, Vol. 21, Oct. 1983, pp. 1448-1452.

[12]Ramkumar, R.L., "Effects of Porosity and Low Velocity Impact Damage on the Strength and Lifetime of Graphite/Epoxy Laminates." Paper presented at Joint PTP-4/5 Workshop on Failure Modes and Nondestructive Evaluation of Composites, Royal Naval Engineering College, Plymouth, England, July 1984.

[13]McCarty, J. and Whitehead, R.S., "Damage Tolerance of Composites Program," Boeing/AFWAL Contract F33615-82-C-3213, Interim Repts. 1-5, Feb. 1983-Feb. 1985.

[14]Ashton, J.E. and Whitney, J.M., *Theory of Laminated Plates*, Technomic, Stanford, CT, 1970.

[15]Jones, R.M., *Mechanics of Composite Materials*, McGraw-Hill, New York, 1975.

[16]Whitney, J.M. and Pagano, N.J., "Shear Deformation in Heterogeneous Anisotropic Plates," *Transactions of ASME, Journal of Applied Mechanics*, Vol. 92, Dec. 1970, pp. 1031-1036.

[17]Mindlin, R.D., "Influence of Rotary Inertia and Shear on Flexural Motions of Isotropic, Elastic Plates," *Transactions of ASME, Journal of Applied Mechanics*, Vol. 73, March 1951, pp. 31-38.

[18]Williams, D., "Dynamic Loads in Aeroplanes Under Given Impulsive Loads with Particular Reference to Landing and Gust Loads on a Large Flying Boat," British Royal Aeronautical Establishment, Repts. SME 3309 and 3316, 1945.

[19]Sanders, W.J., "Computation of Natural Frequencies of Clamped Laminated Plates Using Lagrangian Multiplier Technique," Master's Thesis, California State University, May 1983.

[20]Ramkumar, R.L., Chen, P.C., and Saunders, W.J., "Free Vibration Solution for Clamped Orthotropic Plates Using Lagrangian Multiplier Technique," *AIAA Journal*, Vol. 25, Jan. 1987, pp. 146-151.

[21]Reed, D.L., "Laminated Sandwich Panel Analysis," General Dynamics, Conair Aerospace Division, Rept. FZM 5590 prepared for U.S. Air Force Materials Laboratory, Oct. 1971.

[22]Northrop-Developed Computer Code based on the structural analysis procedure in Ref. 21.